2026 IEEE/SICE International Symposium on System Integration (SII)
January 11-14, 2026. Cancún, México

On Predictive Operation of Hybrid Dynamical Adsorption Cooling Facade Systems*

Melanie Gschweng[1], Olaf Böckmann[2], Micha Schäfer[2] and Oliver Sawodny[1]

Abstract— **Sustainable cooling is an increasingly important part of meeting the cooling demand for thermal comfort in buildings. Adsorption cooling facade systems (ACFS) are one approach to address this by utilizing solar energy on the buildings facade for sustainable indoor cooling. The ACFS' cooling potential is provided by a facade-integrated adsorption-desorption cycle, driven by solar irradiation. The performance of the hybrid nonlinear system highly depends on ambient conditions. To efficiently operate the system, an operational strategy is necessary. This paper proposes a model-based operational strategy using optimal control. The evaluation shows a performance improvement by up to 45 % for the temperature peak overshoot above the target value compared to the rule-based operation.**

I. Introduction

Heat waves and rising ambient air temperatures are projected to triple the energy demand for space cooling in the European Union from 2015 to 2050 [1]. Therefore, sustainable solutions are essential to meet the growing cooling demand. A system class that addresses this challenge are sorption-systems. In this work, we focus on adsorption cooling facade systems (ACFS), that include a single adsorber and the working pair water and zeolite 13X [2], [3]. These systems utilizes solar irradiation on building facades as driver of the desorption process that directly generates and stores cooling potential in the facade component. By the time shifted adsorption process, the cooling capacity is introduced into the room via an evaporator.

Optimization frameworks are frequently used for optimal operation of thermal systems in order to minimize costs for air conditioning or produced emissions. Within those frameworks, applied methods range from constraint optimization [4], (mixed-integer) linear and nonlinear programming [5]–[7] to model predictive control [4], [7], [8]. A reason for this range lies within decomposing the overall problem into sub-problems. This decomposition allows the use of several solution methods, each tailored to the specific characteristics of the corresponding sub-problem. In [7], the sub-problems follow a hierarchical order, representing a supervisor that utilizes weather forecasts to estimate the required heating demand, a reference-tracking part and a hardware-control.

Papageorgiu et al. [9] present an optimization framework for hybrid systems that utilizes a decomposition in two sub-problems. First, the sequence of discrete modes is determined, followed by the optimization with respect to switching surfaces, conditions, and associated costs.

While the ACFS directly stores cooling potential in the adsorber, the sorption-based cooling system studied by Bau et al. [8] includes thermal baths as energy storage. The temperatures of the sorption cycles main components are set with water from the thermal baths. Through this influence, they optimize the phase time of the adsorption-desorption cycle process with nonlinear model predictive control and thereby increase the specific cooling power by 31.1 %. Even though nonlinear optimization poses as promising approach, the strategy from [8] can not directly be transferred to the ACFS. The design of the ACFS without additional thermal water reservoirs increases the system's dependence on ambient conditions and presents additional challenges to the operational strategy, such as deviations from the typical operation cycle. For instance, on a warm but cloudy day, solar irradiation may be insufficient to start desorption, resulting in its omission from the cycle.

We apply the approach from [9] to the hybrid ACFS for the design of a predictive operational strategy. Therefore, the overall problem is split in two parts. A sequence generation step to determine the order of the discrete system states, followed by an optimization step to compute the corresponding switching times. Compared to the rule-based strategy, the predictive strategy promises performance improvements through optimization, as shown in [8]. The main contribution is a model-based operational strategy for the hybrid ACFS.

The work is structured as follows. Section II gives a very brief overview of the ACFS' model. Sequence generation and optimal control for the system are specified in Section III. The simulation model of the ACFS including subordinate component controller and supervisor for discrete state transitions are taken from [2], [10] (cf. Fig. 1). The evaluation procedure and results are discussed in Sections IV and V, respectively. Section VI provides a conclusion and outlook.

II. Modeling Principles of the ACFS

This section briefly summarizes the key concepts of the ACFS' dynamic model. Interested readers can find a detailed explanation of the ACFS, the dynamical model and the rule-based strategy in [2].

*Funded by the Deutsche Forschungsgemeinschaft (DFG, German Research Foundation) - Project-ID 279064222 - CRC 1244, B04, C06

[1]Melanie Gschweng and Oliver Sawodny are with the Institute for System Dynamics, University of Stuttgart, Stuttgart, Germany {melanie.gschweng, sawodny}@isys.uni-stuttgart.de

[2]Olaf Böckmann and Micha Schäfer are with the Institute for Building Energetics, Thermotechnology and Energy Storage University of Stuttgart, Stuttgart, Germany {boeckmann, schaefer}@igte.uni-stuttgart.de

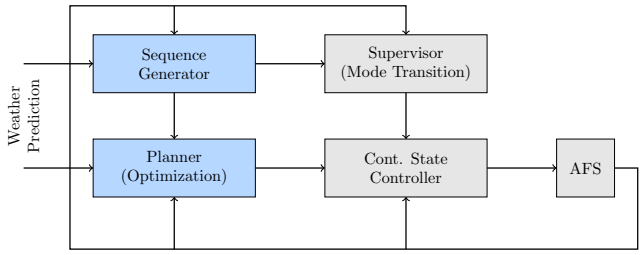

Fig. 1: Block structure of the operational setup. Gray boxes indicate the components of the simulation model from previous works [2], [3], [10]. Blue boxes represent the two parts of the predictive strategy from Sec. III.

The ACFS yields a hybrid system model that integrates continuous and discrete-state dynamics, called modes, to capture the behavior of the solar driven adsorption-desorption cycle. The system consists of an adsorber (A), a condenser (C) and an evaporator (E) as individual components that are mounted to a room (R). The components A/C/E can be deliberately coupled or decoupled to transition between the discrete modes of the sorption cycle. The set $\mathcal{Q} = \{1, 2, ..., 5\}$ refers to the five discrete modes with the following mapping: 1 Inter-Heating (IH), 2 Regenerating (Reg), 3 Inter-Cooling (IC), 4 Cooling (C), 5 Pumping (P). For each $q \in \mathcal{Q}$ the continuous dynamic of state $\boldsymbol{x} \in \mathbb{R}^{12}$, input $u \in \mathbb{R}$, and disturbance $\boldsymbol{z} \in \mathbb{R}^5$ is given by

$$\begin{aligned} \dot{\boldsymbol{x}} &= \boldsymbol{f}_q(\boldsymbol{x}, u, \boldsymbol{z}, t), \\ \boldsymbol{x} &= \begin{bmatrix} T_\mathrm{A} & T_\mathrm{C} & T_\mathrm{E} & X_\mathrm{A} & m_\mathrm{C} & m_\mathrm{E} & \boldsymbol{T}_{1-5} & T_\mathrm{R} \end{bmatrix}, \\ \boldsymbol{z} &= \begin{bmatrix} T_\mathrm{amb} & \dot{\boldsymbol{q}}_\mathrm{sol} \end{bmatrix}. \end{aligned} \tag{1}$$

The state $\boldsymbol{x}$ contains component temperatures $T_{\mathrm{A/C/E}}$, water masses $m_{\mathrm{C/E}}$, room temperature T_R, and temperatures $\boldsymbol{T}_{1-5}$ of the adjacent wall and insulation layers. The adsorber water uptake $X_\mathrm{A} = {}^{m_\mathrm{A}}/_{m_\mathrm{zeo}}$ is the adsorbed water mass m_A per mass of dry zeolite m_zeo. The dynamical equations for the ACFS' components can be found in [2], differential equation for room, wall and insulation temperatures in [10]. Pressures $p_{\mathrm{A/C/E}}$ within the three components are assumed to correspond to the saturation vapor pressures of water and are integrated as algebraic equations. The disturbances are the ambient temperature T_amb and the solar irradiation $\dot{\boldsymbol{q}}_\mathrm{sol} \in \mathbb{R}^4$ on vertical surfaces oriented towards four cardinal directions. The input u sets the water vapor flow from evaporator to adsorber according to [10] via an opening frequency of a connection valve. This vapor flow initiates cooling of the evaporator and the adjacent room during system mode Cooling (C). Therefore, $u \equiv 0\,\mathrm{Hz}$ applies for all other modes (IH, IC, Reg, P).

III. Operational Strategy

This section focuses on the operational strategy of the hybrid system. Analogous to [9], we distinguish between the finite sequence of modes (Sec. III-A) and the subsequent optimization (Sec. III-B), cf. Fig. 1.

A. Sequence Generator

The system cannot switch between adsorption and desorption arbitrarily, as the transitions strongly depend on surrounding conditions, like solar irradiation. The sequence generator exploits this restriction and combines it with knowledge about the sorption cycle of the ACFS to generate a sequential arrangement of the system modes. The resulting sequence $\mathcal{S}$ is built from the tuples $\mathcal{S}_\mathrm{Reg} = \{(1, 2)\}$, $\mathcal{S}_\mathrm{C} = \{(3, 4)\}$, and $\mathcal{S}_0 = \{(3)\}$, which are selected and ordered by the sequence generator with respect to expected ambient conditions. The tuples consider that the goal of mode 1 (IH) is to prepare the system to start regenerating (the desorption process) with mode 2. Likewise, the goal of mode 3 (IC) is to prepare the system to start cooling (adsorption), mode 4. The intermediate modes, IH and IC, may be skipped in some cases which is resolved by the predictive planner from Sec. III-B.

Mode 5, pumping, can be performed at any point in the sequence and takes comparatively short time (about 10 minutes). Therefore we assume that the decision to start mode 5 is made by the supervisor and continuous state controller (cf. Fig. 1). Inter-Cooling, mode 3, is used as default tuple $\mathcal{S}_0$ at the start and end of the sequences, as well as between the tuples.

The generator arranges the tuples for cooling and regeneration through numerically integrating subsystems with approximated weather conditions. In both cases, the time spans during which the ACFS is likely able to cool or regenerate are determined by evaluating the required pressure conditions for adsorption and desorption, respectively. Time periods during which the corresponding pressure condition is met are labeled as periods with potential for regeneration or cooling. The starting times of these periods indicate the order of the tuples. Both subsystems and required pressure conditions are given in the following.

1) Desorption periods: Time intervals with expected regeneration potential must fulfill the pressure condition

$$p_A(T_A, X_A) > p_C(T_C), \tag{2}$$

while the adsorber is heated by solar irradiation. The subset of adsorber and condenser temperatures with the dynamics of mode 1, Inter-Heating, is sufficient to estimate time periods where the system can regenerate. The governing dynamical equations are

$$\begin{aligned} \dot{T}_\mathrm{A} &= \frac{1}{m_\mathrm{A} c_{\mathrm{zeo,water}}(T_\mathrm{A})) + k_\mathrm{A}} \dot{Q}_{\mathrm{A},1}(T_\mathrm{A}, t) \\ \dot{T}_\mathrm{C} &= \frac{1}{m_\mathrm{C} c_{\mathrm{water}}(T_\mathrm{C})) + k_\mathrm{C}} \dot{Q}_\mathrm{C}(T_\mathrm{C}, t), \end{aligned} \tag{3}$$

with $\dot{Q}_{\mathrm{A},1/\mathrm{C}}$ as the resulting heat fluxes between component and ambiance that utilize differentiable approximations of ambient temperature and solar irradiation, constants $k_{\mathrm{A/C}}$ that summarize material properties from [2], specific heat capacity $c_{\text{zeo,water}}$ from [11], and specific heat capacity of water c_{water} according to [12]. The states representing the water masses $m_{\mathrm{A/C}}$ are constant in mode 1.

2) Adsorption periods: Time intervals with expected cooling potential must fulfill

$$p_A(T_A, X_A) < p_E(T_E). \tag{4}$$

The dynamical model

$$\begin{aligned} \dot{T}_\mathrm{A} &= \frac{1}{m_\mathrm{A} c_{\mathrm{zeo,water}}(T_\mathrm{A})) + k_\mathrm{A}} \dot{Q}_{\mathrm{A},3}(T_\mathrm{A}, t) \\ \dot{T}_\mathrm{E} &= \frac{1}{m_\mathrm{E} c_{\mathrm{water}}(T_\mathrm{E})) + k_\mathrm{E}} \dot{Q}_\mathrm{E}(T_\mathrm{E}, T_\mathrm{R}, t), \end{aligned} \tag{5}$$

represents the subset of adsorber and evaporator temperatures during the mode Inter-Cooling. Analog to (3), $\dot{Q}_{\mathrm{A},3/\mathrm{E}}$ are the resulting heat fluxes between component and ambiance that utilize differentiable approximations of ambient temperature and solar irradiation, k_E summarizes material properties from [2], and water masses $m_{\mathrm{A/E}}$ are constant. Instead of integrating a dynamic model of the room temperature, (5) is evaluated for two cases. Case 1 approximates T_R with the approximated ambient temperature $\tilde{T}_\mathrm{amb}$, and represents a scenario with high air circulation in the room. Case 2 utilizes a predefined constant lower bound $T_{\mathrm{R,min}}$ to approximate the room temperature.

B. Predictive Planner

The predictive planner sets up and numerically solves an optimal control problem over the fixed time period of a single day and thereby switches between the discrete system modes according to the sequence $\mathcal{S}$. The nonlinear optimization problem for operating the hybrid system is

$$\begin{aligned} \min_{\tilde{u}(t^*), \phi(t^*)} \; & \{J(\tilde{\boldsymbol{x}}, t^*) \,|\, \dot{\tilde{\boldsymbol{x}}} = \tilde{f}_{\phi(t^*)}(\tilde{\boldsymbol{x}}, \tilde{u}, \tilde{\boldsymbol{z}}, t^*), \\ & \tilde{\boldsymbol{x}}(0) = \tilde{\boldsymbol{x}}^0 \\ & \tilde{\boldsymbol{x}}_\mathrm{min} \leq \tilde{\boldsymbol{x}} \leq \tilde{\boldsymbol{x}}_\mathrm{max} \\ & \boldsymbol{g}_{\phi(t^*)}(\tilde{\boldsymbol{x}}, \tilde{u}, t^*) \leq \boldsymbol{0}\}, \end{aligned} \tag{6}$$

with

$$\tilde{\boldsymbol{x}} = \begin{bmatrix} \Delta t_j^* & T_\mathrm{A}^* & T_\mathrm{C}^* & T_\mathrm{E}^* & X_\mathrm{A}^* & \boldsymbol{T}_{1-5}^* & T_\mathrm{R}^* \end{bmatrix} \tag{7}$$

utilizing scaled entities (denoted with *) according to $\xi^* = \xi / \xi_{ref}$ with separate reference values for times t_ref, temperatures T_ref and water uptake levels X_ref to enhance convergence to the optimal solution. In (6) and (7), Δt_j, $j = 1, .., n_p$ are non-negative time intervals for each of the n_p modes in $\mathcal{S}$, $\phi(t) = s_j$ is a piece wise constant function for $\sum_{m=0}^{j-1} \Delta t_m < t \leq \sum_{m=0}^{j} \Delta t_m$ with $\Delta t_0 = 0\,\mathrm{s}$ and $s_j \in \mathcal{Q} \setminus \{5\}$, $\tilde{\boldsymbol{x}}^0$ is the initial condition, $\tilde{\boldsymbol{x}}_\mathrm{min}$ and $\tilde{\boldsymbol{x}}_\mathrm{max}$ are lower and upper limits, respectively, and $\boldsymbol{g}_{\phi(t^*)}(\tilde{\boldsymbol{x}}, \tilde{u}, t^*)$ represents state depended (in-)equality constraints.

The differential equations of each mode in (6) are based on the dynamics from (1) with $\Delta \dot{t}_j^* = 0$ for all $j = 1, ..., n_p$. In $\tilde{f}$, the state depending adsorption enthalpy and diffusion coefficient of Knudsen-Diffusion are fixed to their average values over the state ranges $X_\mathrm{A} \in [0.2, 0.3]$ and $T_\mathrm{A} \in [0\,^\circ\mathrm{C}, 150\,^\circ\mathrm{C}]$ to reduce the model complexity and improve the convergence of the numerical optimization. The adsorbers plate fins efficiency is approximated with 1 since state depended values lie in $[0.9992, 1.0004]$. Water masses in evaporator and condenser are treated as constant parameters over the course of one optimization to reduce the dimensionality of the problem and the number of constraints. Disturbances $\tilde{\boldsymbol{z}}$ are the differentiable approximations of $\boldsymbol{z}$, input $\tilde{u}$ directly sets the vapor mass flow from evaporator to adsorber. Utilizing the input in the proposed way renders the optimization problem independent of the actual connection of evaporator and adsorber from [2], [3], [10].

The objective function $J(\tilde{\boldsymbol{x}}, t^*)$ combines the goals of maintaining the desired room temperature $\hat{T}_\mathrm{R}$ and restoring the cooling potential by reducing the adsorber uptake during regeneration,

$$\begin{aligned} J(\tilde{\boldsymbol{x}}, t^*) = \theta_\mathrm{T} T_\mathrm{ref}^2 t_\mathrm{ref} \int_0^{t_f^*} (T_\mathrm{R}^* - {}^{\hat{T}_\mathrm{R}}/_{T_\mathrm{ref}})^2 dt^* \\ + \theta_\mathrm{X} X_\mathrm{ref} \underbrace{\int_0^{t_f^*} \sum_{i=1}^{n_\mathrm{Reg}} (H(t^* - t_{\mathrm{Reg}0}^{*i}) - H(t^* - t_{\mathrm{Reg}f}^{*i})) \dot{X}_\mathrm{A}^* dt^*}_{= \sum_{i=1}^{n_\mathrm{Reg}} \left(X_\mathrm{A}^*(t_{\mathrm{Reg}f}^{*i}) - X_\mathrm{A}^*(t_{\mathrm{Reg}0}^{*i}) \right)}, \end{aligned} \tag{8}$$

with Heaviside step function H, $n_\mathrm{Reg} \in \mathbb{N}$ as number of mode regenerating in $\mathcal{S}$, and $t_{\mathrm{Reg}0}^i$ and $t_{\mathrm{Reg}f}^i$ as start and end times of regeneration[1]. Both goals are weighted according to constant θ_T and piece wise constant θ_X with $\theta_\mathrm{X} = 0$ when $2 \notin \mathcal{S}$, i.e., not regenerating. This trade-off between the two goals is essential to ensure the continuation of the cyclic adsorption-desorption process since regeneration reduces the adsorber water uptake, i.e., restores the cooling potential of the ACFS. Without addressing this objective, the system tends towards a system state that does not allow further cooling.

Physical feasibility is addressed through mode depended (in-)equality constraints and state limits. The time intervals are subjects to

$$\sum_{j=1}^{n_p} \Delta t_j^* = t_f^*, \tag{9}$$

to ensure that the mode sequence spans over the complete time horizon. The state constraints are

$$T_\mathrm{E} \geq \hat{T}_{\mathrm{E,min}} \tag{10a}$$

$$p_\mathrm{E}(T_\mathrm{E}(\mathbf{t}_\mathrm{C0})) \geq p_\mathrm{A}(T_\mathrm{A}, X_\mathrm{A})|_{\mathbf{t}_\mathrm{C0}} \tag{10b}$$

$$0\,{}^\mathrm{kg}/_s \leq \tilde{u}(t) \leq u_\mathrm{max} \tag{10c}$$

for $\phi(t) = 4$ (Cooling) with desired minimum evaporator temperature $\hat{T}_{\mathrm{E,min}}$, while $\tilde{u}(t) = 0\,{}^\mathrm{kg}/_s$ for $\phi(t) \neq 4$, and

$$\dot{X}_\mathrm{A} \leq 0 \tag{11a}$$

$$\dot{T}_\mathrm{A} \geq 0 \tag{11b}$$

$$p_\mathrm{C}\left(T_\mathrm{C}(\mathbf{t}_{\mathrm{Reg}0})\right) \leq p_\mathrm{A}(T_\mathrm{A}, X_\mathrm{A})|_{\mathbf{t}_{\mathrm{Reg}0}} \tag{11c}$$

for $\phi(t) = 2$ (Regenerating). To scale the constraints, reference pressure p_ref and input $u_\mathrm{ref} = u_\mathrm{max}$ are used.

[1]Compared to [9], the integral formulation for the regenerating objective can be interpreted as running costs, whereas the summation formulation corresponds to switching costs.

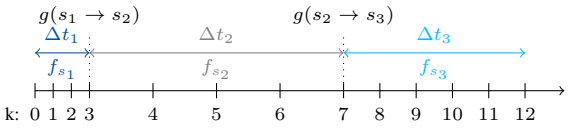

Fig. 2: Discretization scheme for a sequence with three modes $s_j \in \mathcal{S}$, $j = 1, 2, 3$ and time points $k = 0, 1, ..., K$ with $K = 12$. If applicable, mode depended pressure conditions (cf. (2) and (4)) are posed at $g(s_j \to s_{j+1})$ for $j = 1, 2$.

Analogous to the transition equality conditions from [9], equations (10b) and (11c) impose state dependent transition conditions from modes 3 to 4 (cf. (4)), and 1 to 2 (cf. (2)). Therefore (10b) and (11c) are posed for all transitions times to modes 2, $\mathbf{t}_{\mathrm{Reg0}}$, and 4, $\mathbf{t}_{\mathrm{C0}}$. Equations (11a) and (11b) preserve pressure conditions during regenerating.

IV. Numerical Methods and Evaluation

We solve problem (6) with IPOPT from [13], using direct collocation with implicit midpoint rule for each 24-hour period, starting and ending at midnight, such that $t_f = 84600\,\mathrm{s}$. The discretization scheme varies dynamically and follows a mode-dependent scheme with a fixed number of grid points per system mode as illustrated in Fig. 2. Interval midpoints $t^{k+1/2} = (t^{k+1} - t^k)/2$ are used as collocation points for $k = 0, 1, ..., K-1$.

Modes 1 to 3 are discretized using four points, whereas mode 4 employs ten points to ensure a sufficiently accurate representation of input $\tilde{u}$ while maintaining a reasonable number of collocation points. Within each mode, the points are equally distributed over the respective time intervals Δt_j for $j = 1, ..., n_p$, leading to variable step sizes during the course of optimization and across different modes (cf. Fig. 2). The scheme of the discretized system dynamics and the collocation conditions can be found in [14].

A. Evaluation

The predictive strategy is compared to the rule-based strategy from [2] using identical initial and ambient conditions. Two perspectives of the predictive strategy are evaluated. First, the solution of the optimal control problems for each individual day (called optimization) and second, continuous simulations based on the solution of the optimization (called tracking). The latter involves tracking the optimized transition times and evaporator temperatures without the simplifications introduced for numerical optimization. Starting from the second day, the initial conditions of the states for the predictive strategy are extracted from the tracking solution of the previous day. The sequence generator provides initial conditions for the time intervals of the modes in the determined sequence $\mathcal{S}$. The system behavior of the rule-based strategy is known to converge to a daily cycle over a series of repetitions of the same day (e.g., [2], [3]). The initial conditions for the conducted study are from the final state of such a steady-state cycle.

B. External Disturbances

As ambient conditions for air temperature and solar irradiation, a summer real week (17.06.2023 - 23.06.2023,

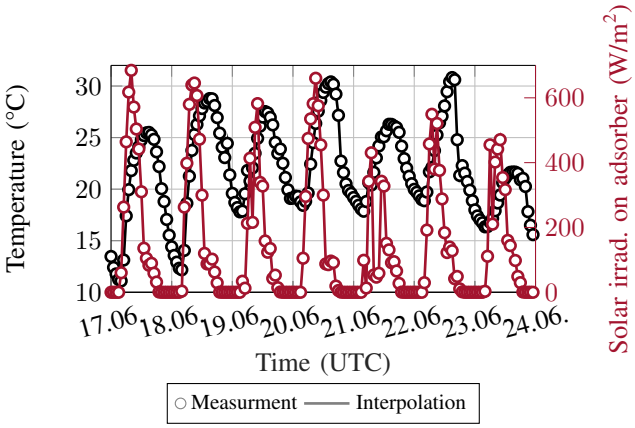

Fig. 3: Ambient temperature and solar irradiation in south east orientation for a summer week from 2023 in Stuttgart [15].

Fig. 3) is extracted from the data source [15]. The data is repeated ten times and concatenated for simulation to allow the system to reach a steady-state cycle, thereby minimizing transient behaviors resulting from initialization. However, for the evaluation, only the 10th repetition is considered.

The selected week is a mixture of warm and hot days, combined with varying levels of sunshine in a Central European representative climate. The hourly data from [15] is linearly interpolated to simulate the ambient conditions. For optimization, a fourth degree polynomial approximates the temperature data of each day. Polynomials of degree six approximate the solar irradiation between sunrise and sunset, with differentiable transitions between daytime and nighttime.

The proposed approximation refers to the hourly data as weather forecast and is transferable to real applications. A prototype of the ACFS is built in Stuttgart, Germany. For this location, the German Weather Service (`https://opendata.dwd.de/`) provides hourly weather data for the next ten days.

V. Simulation Results and Discussion

The presented results illustrate the behavior of the ACFS and its influence on the room temperature. The areas of evporator, condenser and adsorber are $1\mathrm{m}^2$ each, the air change rate between ambiance and room is 2 per hour. The room has lightweight walls with parameters from [16] and a size of 1 m x 1 m x 2.4 m so that the evaporator covers the entire ceiling. Other parameters are listed in Tab. I.

Figure 4 illustrates the temperatures of the ACFS components and the room, as well as the water uptake of the adsorber for $\hat{T}_{\mathrm{R}} = 20\,°\mathrm{C}$ and $\hat{T}_{\mathrm{E,min}} = 15\,°\mathrm{C}$. The predictive strategy maintains the temperature near the target value as good as (or slighty better than) the rule-based strategy while storing, in average, an increased cooling potential. Neither strategy is able to maintain the target value for the entire week. This limitation arises from the system design with

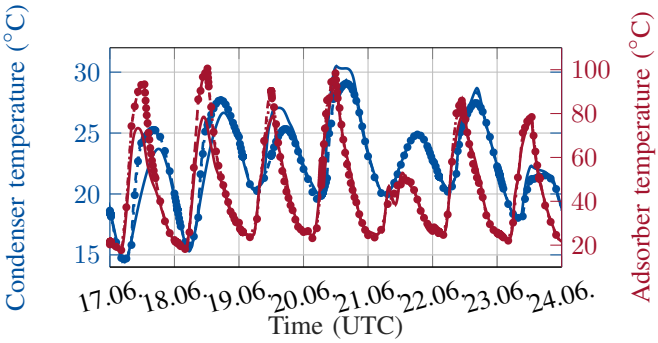

(a) Adsorber and condenser temperatures.

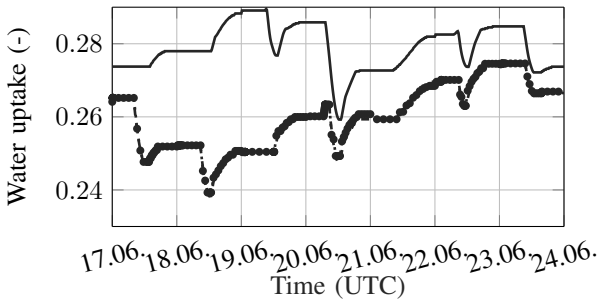

(b) Adsorber water uptake, decreases during regeneration (desorption) and increases during cooling (adsorption).

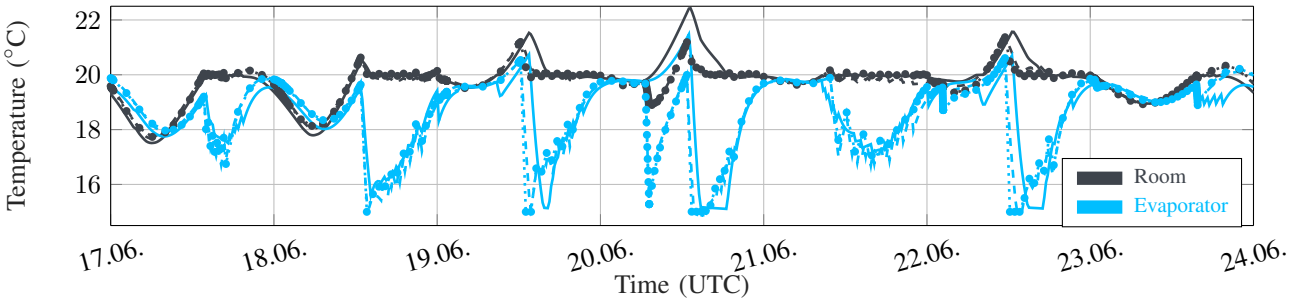

(c) Room and evaporator temperatures. Evaporator temperatures below room temperatures imply cooling.

Optimization Tracking Rule-based

Fig. 4: System behavior for the rule-based strategy and both perspectives of the predictive strategy (referred to with optimization and tracking).

a single adsorber[2] in combination with the dependence on ambient conditions for mode transitions and the absence of a heating source. Therefore, deviations are acceptable, while minimizing temperature rises above the target value is a key objective. The predictive strategy reduces the maximum exceeding of the desired room temperature by 1.09 °C compared to the rule-based strategy which equals a peak reduction by around 45 %.

Taking into account predictive information about the course of the day enables a more effective operation of the system, as demonstrated by the behavior on June 20. Given the expected ambient conditions, the predictive strategy employs two cooling phases with regeneration in between, while the rule-based approach uses one cooling phase. The additional cooling phase around 6:30-7:00 reduces the room temperature below the target temperature, which minimizes both the maximum and average deviation from the target value throughout the day.

The proposed strategy decreases the average deviation from the desired room temperature to approx. 0.44 °C for optimization and 0.62 °C for tracking. The average deviation with the rule-based strategy is slightly higher with 0.68 °C. Differences between tracking and optimization arise due to temperature drops around 0.1 °C to 0.3 °C below the target temperature during tracking. This appears especially during time periods, where the optimization approximately keeps the target temperature, e.g., June 18, 14:00-21:00 or June, 21, from 11:00 (Fig. 4c). Using the optimization results as feed forward control overestimates the necessary cooling demand. Two reasons arise from differences in the disturbance estimation and due to the evaporator temperature control from [10]. June 21st has the largest fluctuations in solar irradiation on the adsorber (see Fig. 3) which leads to differences in the adsorber temperature between tracking and optimization. This difference may indirectly influence the provided cooling demand. In addition, the controller for the water flow from evaporator to adsorber is directly taken from [10] without adjustments. However, the evaporator temperature tracking performance is not ideal. This leads to a temperature below the optimized evaporator temperature and increases the cooling capacity. Future applications must be equipped with a room temperature control in order to compensate for unexpected disturbances, such as lengthening of meetings. Combining this controller with an improved evaporator temperature reference tracking should minimize the deviations of the room temperature. The average adsorber water uptake lies around 0.248 and 0.281 for predictive and rule-based strategy, respectively (cf. Fig. 4b). This reduced uptake of the predictive strategy implies additional cooling potential which results from superior desorption (regeneration of the adsorber) or increased efficiency during cooling (adsorption).

Observable adsorber and condenser temperature differ-

[2]The first prototype of the ACFS uses this design and focuses on demonstrating the overall principle. Planned research projects will address multi-adsorber systems to overcome this limitation.

ences in Fig. 4a between the strategies result from varying sequences of the system modes. For June 17 and 18, only the predictive strategy includes the system modes 1 and 2, e.g., tuple $\mathcal{S}_{\mathrm{Reg}}$, in the transition sequence. Thus, compared to the rule-based strategy, the adsorber temperature increases during Inter-Heating, mode 1, and the condenser temperature increases during regeneration. This also implies that the rule-based strategy does not regenerate during those two days as seen in Fig. 4b.

Due to the nonlinear dynamic of the ACFS, the optimization process may struggle to find the optimal solution. In such cases, it oscillates around a potential minimum without converging to it and terminates after 3000 iterations. In Fig. 4, four days fall into this category. For two of the 70 days, the optimization converged to an infeasible solution, where the rule-based strategy is used as a fallback. The convergence problems result from the trade-off between the two objectives and the interaction with the pressure constraints. Reformulating the optimization problem could guarantee convergence but would require model simplifications. Linearizing around a trajectory presents a promising approach to improve the numerical stability of the optimization problem.

VI. Conclusion

This study presented an optimal operation strategy for a hybrid sorption system. Daily operation is split in two parts: A sequence generator to sort the discrete system modes and a subsequent optimal control problem. A tracking setup uses the optimization results as feed forward control for the original simulation model of the ACFS. The predictive strategy improves efficiency of the single-adsorber-design facade system by increasing the average amount of stored cooling potential while minimizing temperature deviations compared to the rule-based strategy. While a rule-based strategy is comparably straightforward for the studied single-adsorber-system, multi-adsorber systems with thermal and material couplings increase the complexity of designing rule-based operational strategies. The proposed design strategy can be adjusted to such systems but will need further refinement to address convergence issues of the nonlinear optimization problem, especially with increasing problem dimensionality through system advances. Future works will therefore study a division of the presented optimal control problem in hierarchical sub-problems, starting with estimations of the cooling demand that lead to reference trajectories for the evaporator temperature. Especially in case of multi-adsorber-systems, those reference trajectories will be then used to determine mode sequences and transition times.

TABLE I: Parameter and Values

	Description	Value	Unit
D_{kn}	Knudsen-Diffusion coef.	$6.3831 \cdot 10^{-05}$	$\mathrm{m^2/s}$
T_{ref}	Temperature scaling coef.	373.15	K
$T_{\mathrm{R,min}}$	Lower bound for room temp.	291.15	K
X_{ref}	Uptake scaling coef.	0.339	-
dt	Simulation step size	60	s
k_A	material prop. from [2]	$1.8115 \cdot 10^5$	$\mathrm{J/K}$
k_C	material prop. from [2]	$2.8816 \cdot 10^5$	$\mathrm{J/K}$
k_E	material prop. from [2]	7290	$\mathrm{J/K}$
p_{ref}	Pressure scaling coef.	$1.0135 \cdot 10^5$	Pa
t_{ref}	Time scaling coef.	86400	s
$u_{\mathrm{ref/max}}$	Input scaling coef.	$0.5 \cdot 10^{-4}$	$\mathrm{kg/s}$
Δh_{A}	Adsorption enthalpy	3076672	$\mathrm{J/kg}$
θ_{T}	Temperature weight	1	$\mathrm{1/K^2 s}$
θ_{X}	Uptake weight during mode 2	10^5	-

References

[1] L. Kranzl, M. Hartner, A. Müller, G. Resch, S. Fritz, T. Fleiter, A. Herbst, M. Rehfeldt, P. Manz, A. Zubaryeva, J. Gómez Vilchez, Hotmaps. Heating & Cooling Outlook Until 2050, EU-28 (2019). doi:10.24406/PUBLICA-625.

[2] J. L. Heidingsfeld, O. Böckmann, M. Schäfer, M. Böhm, O. Sawodny, Low Order Hybrid Model for Control Design of an Adsorption Facade System for Solar Cooling, in: Conf. on Control Technology and Applications, IEEE, 2022. doi:10.1109/ccta49430.2022.9965991.

[3] O. Böckmann, D. Marmullaku, M. Schäfer, Dynamic Modeling and Simulation of a Facade-Integrated Adsorption System for Solar Cooling of Lightweight Buildings, Energies (2024). doi:10.3390/en17071706.

[4] J. Wang, W. Deng, C. Yue, W. Su, X. Bai, Joint Optimization of Cooling Parameters and Workload Distributions based on Model Predictive Control for Rack-based Data Centers, Journal of Building Engineering (Apr. 2025). doi:10.1016/j.jobe.2025.111801.

[5] J. Jansen, F. Jorissen, L. Helsen, Mixed-integer non-linear Model Predictive Control of District Heating Networks, Applied Energy (2024). doi:10.1016/j.apenergy.2024.122874.

[6] R. Padullés, M. L. Hansen, M. P. Andersen, B. Zühlsdorf, J. K. Jensen, B. Elmegaard, Optimal Operation of Industrial Heat Pumps with Stratified Thermal Energy Storage for Emissions and Cost Reduction using Day-ahead Predictions, Applied Thermal Engineering (2025). doi:10.1016/j.applthermaleng.2025.125703.

[7] S. Thorsteinsson, A. A. S. Kalaee, P. Vogler-Finck, H. L. Stærmose, I. Katic, J. D. Bendtsen, Long-term Experimental Study of Price Responsive Predictive Control in a Real Occupied Single-family House with Heat Pump, Applied Energy (2023). doi:10.1016/j.apenergy.2023.121398.

[8] U. Bau, N. Baumgärtner, J. Seiler, F. Lanzerath, C. Kirches, A. Bardow, Optimal Operation of Adsorption Chillers: First Implementation and Experimental Evaluation of a Nonlinear Model-predictive-control Strategy, Applied Thermal Engineering (2019). doi:10.1016/j.applthermaleng.2018.07.078.

[9] M. Papageōrgiu, M. Leibold, M. Buss, Optimierung, 3rd Edition, Springer Berlin Heidelberg, Berlin, Heidelberg, 2012, Ch. 10.6.

[10] M. Gschweng, J. L. Heidingsfeld, O. Böckmann, M. Schäfer, M. Böhm, O. Sawodny, Evaporator Temperature Control of a Solar-Powered Adsorption Facade System, in: Conf. on Control Technology and Applications, IEEE, 2024. doi:10.1109/ccta60707.2024.10666605.

[11] B. Mette, H. Kerskes, H. Drück, H. Müller-Steinhagen, Experimental and Numerical Investigations on the Water Vapor Adsorption Isotherms and Kinetics of Binderless Zeolite 13X, International Journal of Heat and Mass Transfer (2014). doi:10.1016/j.ijheatmasstransfer.2013.12.061.

[12] P. Stephan, S. Kabelac, M. Kind, D. Mewes, K. Schaber, T. Wetzel (Eds.), VDI-Wärmeatlas, 12. edition, Springer Berlin Heidelberg, 2019.

[13] J. A. E. Andersson, J. Gillis, G. Horn, J. B. Rawlings, M. Diehl, Casadi: a software framework for nonlinear optimization and optimal control, Mathematical Programming Computation (Jul. 2018). doi:10.1007/s12532-018-0139-4.

[14] O. von Stryk, Numerische Lösung optimaler Steuerungsprobleme: Diskretisierung, Parameteroptimierung und Berechnung der adjungierten Variablen, in: Fortschr.-Ber. VDI, Reihe 8, Nr. 441. Düsseldorf, https://www.sim.informatik.tu-darmstadt.de/publ/download/1994-diss.html, 1994.

[15] European Commission, Photovoltaic Geographical Information System, https://re.jrc.ec.europa.eu/pvg tools/en/ [accessed: 09.01.2025].

[16] S. O. Weber, O. Böckmann, A. Greiner, S. Park, M. Schäfer, Optimal Conceptual Design of a Novel Facade-Integrated Adsorption Cooling System, in: Proceedings of EuroSun, 2022. doi:10.18086/eurosun.2022.06.11.